Drying of salt solutions in porous materials: Intermediate-time dynamics and efflorescence

Laura Guglielmini,[1] Alexandre Gontcharov,[1] Antonio J. Aldykiewicz, Jr.,[2] and Howard A. Stone[1]
[1]*SEAS, Harvard University, Cambridge, Massachusetts 02138, USA*
[2]*Grace Construction Products, Cambridge, Massachusetts 02140, USA*

(Received 21 March 2008; accepted 2 June 2008; published online 8 July 2008)

Drying of salt solutions leads to the accumulation of salt at any surface where evaporation occurs. When this drying occurs within porous media, the precipitation of salts or efflorescence is generally to be avoided. A one-dimensional model for the drying processes in initially saturated porous materials was presented by Huinink *et al.* [Phys. Fluids **14**, 1389 (2002)] and analytical results were obtained for short times when the concentration distribution evolves diffusively. Here, we present analytical results for intermediate times when convective and diffusive fluxes balance. Moreover, the approach is extended to symmetrical geometries and is generalized for porous objects with arbitrary shape, which highlights the role of the surface area to volume ratio. Estimates for the Peclet number dependence of the maximum salt concentration at the surface are obtained and the conditions that allows to avoid efflorescence are characterized. © *2008 American Institute of Physics*. [DOI: 10.1063/1.2954037]

I. INTRODUCTION

Efflorescence in common masonry materials results in both visual discoloration via streaks, stains, or a uniform haze on the surface and the possible physical deterioration of the material as additional sources of internal stress occur. The efflorescence processes refer to the evaporatively driven transport of soluble salts, such as hydroxides, carbonates, or sulfates from the interior of the masonry to its surface, where precipitation of insoluble salt oxides takes place. In order to describe such processes it is necessary to understand the flow of liquids in porous media and analyze the convective and diffusive processes that transport solutes.

In recent literature, there have been a number of studies focusing on ion transport in evaporating systems and several studies with direct application to efflorescence.[1–7] Results have highlighted the importance of a dimensionless parameter, an effective Peclet number, defined as $\mathrm{Pe}=jL/(\rho\epsilon D^*)$, where j is the evaporation rate, L is the depth of the drying section, ϵ is the porosity, ρ is the density of the liquid, and D^* is the effective diffusion coefficient of the salt in the porous material. For small Peclet numbers, $\mathrm{Pe}<1$, chemical diffusion is most important and the salt concentration is nearly uniform throughout the material; while for $\mathrm{Pe}>1$, advection is most important and the salt ions accumulate at the interface where drying occurs (e.g., Refs. 3, 5, and 7). Various one-dimensional (1D) results have been obtained, and NMR measurements have validated some of the basic predictions,[4] especially those coupling moisture content with the ion concentration profile near the drying interface. When the salt concentration exceeds equilibrium saturation values, precipitation of salt is expected.

In this paper, we build upon the 1D model introduced by Huinink *et al.*[3] for the study of the drying of a rectangular porous medium initially saturated with a salt solution and under conditions where the evaporation rate is constant. These authors presented numerical results for a wide range of Peclet numbers and obtained analytical results for the salt concentration at early times, when the concentration distribution evolves diffusively. Here, we utilize the same model and present analytical results valid for intermediate times, when convective and diffusive fluxes balance. In particular, we determine the spatial structure of the salt profile along the sample, and we provide estimates for the time and Peclet number dependence of the maximum salt concentration. The same approach is applied to other symmetrical objects (cylinders and spheres) and extended, with approximate arguments, to objects of arbitrary shape. Thus, a reasonably general characterization of drying in the intermediate-time regime is obtained.

II. DRYING OF 1D OR SYMMETRICAL SAMPLES

A. Problem formulation

The basic problem formulation for 1D drying of an initially liquid-saturated porous medium has been given by Huinink *et al.*[3] and we refer the reader to their paper for details. We summarize the most important aspects here, with reference to the rectangular geometry of Fig. 1(a). We consider a sample of homogeneous material of length L and uniform porosity ϵ, initially saturated with water, which contains some dissolved salts. The sample undergoes drying as a result of convection of air along its free surface ($z=0$). The other boundaries are impermeable surfaces. We neglect thermal effects and consider one species of salt dissolved in the water; ions do not absorb at the pore walls and we do not account for any dissolution of the material.

In general, the liquid distribution within the porous sample during drying depends on the competition between capillary, viscous, and possibly gravitational forces. A num-

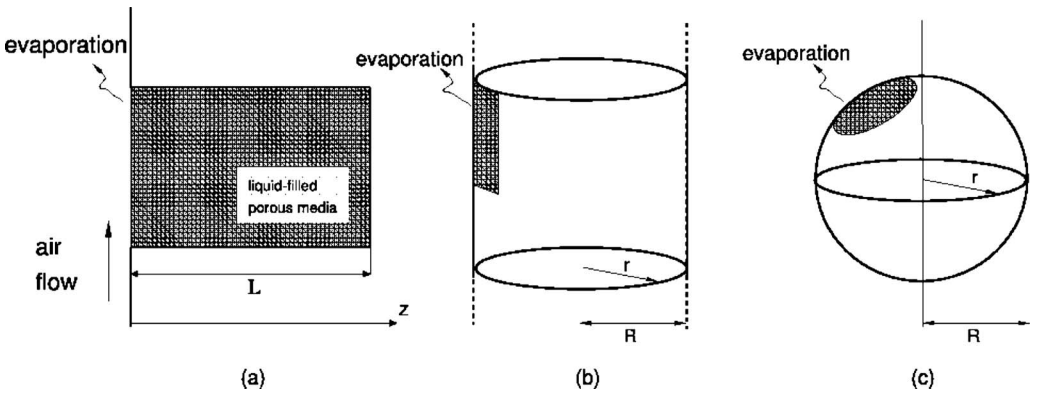

FIG. 1. Schematic of the convective drying of a porous medium of (a) rectangular shape with constant cross section, (b) cylindrical shape with constant cross section, and (c) spherical shape.

ber of recent works, whose results are reviewed in Ref. 8, analyze by means of experiments and comprehensive numerical studies the effect on drying (without consideration of the salt distribution) of gravity[9,10] and viscous effects.[10–12] We will assume that the size of the sample and the characteristic scale of the pores are such that capillary effects are dominant,[7,8,13] in which case it is possible to identify three distinct drying regimes: A *constant rate period*, where the evaporation rate is constant and is determined by the diffusion of vapor in the boundary layer along the free surface of the sample; a falling rate period, during which the decreasing evaporation rate is controlled by the transport of liquid through the porous medium and a dry region invades the interior of the sample; lastly, a receding regime, in which the liquid no longer moves toward the surface and evaporates when the drying front arrives. In this work, we study the constant evaporation rate period and we assume that the liquid saturation S (volume of liquid per available pore volume) is spatially uniform but time varying. This drying regime, discussed in Refs. 8 and 13 and described by means of three-dimensional numerical simulation in Ref. 14 and experiments,[4] extends down to saturations in the range $S=0.3-0.4$.[7]

The 1D equation that governs ion transport in the liquid confined to a porous media is

$$\frac{\partial(\rho\epsilon SC)}{\partial t}=\frac{\partial}{\partial z}\left(\rho\epsilon SD^*\frac{\partial C}{\partial z}-\rho\epsilon SCU\right), \tag{1}$$

where C is the mass fraction of salt dissolved in the liquid phase, ρ is the density of the solution, which for simplicity is assumed constant and is independent of the salt concentration, U is the average velocity of the liquid, and D^* is the effective diffusion coefficient for the dissolved salt. The boundary conditions at $z=0$ and $z=L$ are obtained by requiring that the diffusive and convective fluxes balance (ions cannot escape from the liquid phase),

$$UC-D^*\frac{\partial C}{\partial z}=0 \quad \text{at} \quad z=0,L, \tag{2}$$

where both terms need to be multiplied by $\rho\epsilon S$ to obtain the fluxes expressed as mass per unit area per time.

For a given constant drying rate j_{cr} (mass per unit area per time), and with the assumption that S is a function of time only, then $j_{cr}=-\rho L\epsilon(dS/dt)$ and $S=1-(j_{cr}/\rho L\epsilon)t$. Furthermore, using a mass balance for the liquid,[3] it follows $U=[j_{cr}/\rho L\epsilon S(t)](z-L)$. Thus, we have all the elements to solve for the salt concentration $C(z,t)$.

B. Dimensionless problem statement

We approximate D^* with its value at saturation, so that the ion-transport equation (1) can be written as

$$\frac{\partial(SC)}{\partial t}=D^*\frac{\partial^2(SC)}{\partial z^2}-\frac{j_{cr}}{\rho L\epsilon-j_{cr}t}\frac{\partial[SC(z-L)]}{\partial z}. \tag{3}$$

The macroscopic problem is characterized by the length scale L (the characteristic scale of the pores does not enter directly), the diffusion time scale $\tau_D=L^2/D^*$, and the convective time scale or drying time $\tau_C=\epsilon L\rho/j_{cr}$. We follow[3] and introduce the dimensionless variables $\tau=tD^*/L^2$, $\zeta=z/L$, and $\Omega=SC/\langle SC\rangle$, where $\langle SC\rangle$ is the integral average of the product SC over the domain. The only dimensionless parameter is the Peclet number,

$$\mathrm{Pe}=\frac{\tau_D}{\tau_C}=\frac{L^2/D^*}{\rho L\epsilon/j_{cr}}=\frac{Lj_{cr}}{\rho\epsilon D^*}. \tag{4}$$

Hence, we now have the dimensionless problem

$$\frac{\partial\Omega}{\partial\tau}=\frac{\partial^2\Omega}{\partial\zeta^2}-\frac{\mathrm{Pe}}{1-\mathrm{Pe}\tau}\left[(\zeta-1)\frac{\partial\Omega}{\partial\zeta}+\Omega\right],$$
$$\frac{\mathrm{Pe}}{1-\mathrm{Pe}\tau}(\zeta-1)\Omega-\frac{\partial\Omega}{\partial\zeta}=0 \quad \text{at} \quad \zeta=0,1, \tag{5}$$

which can be solved numerically.

Typical numerical results have already been provided in Refs. 3 and 7. Both of these references highlight the effect on the ion distribution of the value of Pe [see Fig. 2(a)]. As already mentioned, for $\mathrm{Pe}\ll 1$ diffusive effects are dominant so that ions remains nearly uniformly distributed throughout the medium. For $\mathrm{Pe}\simeq 1$, we observe a crossover behavior and there is accumulation of ions in the region close to the free surface where evaporation occurs. For $\mathrm{Pe}\gg 1$, convec-

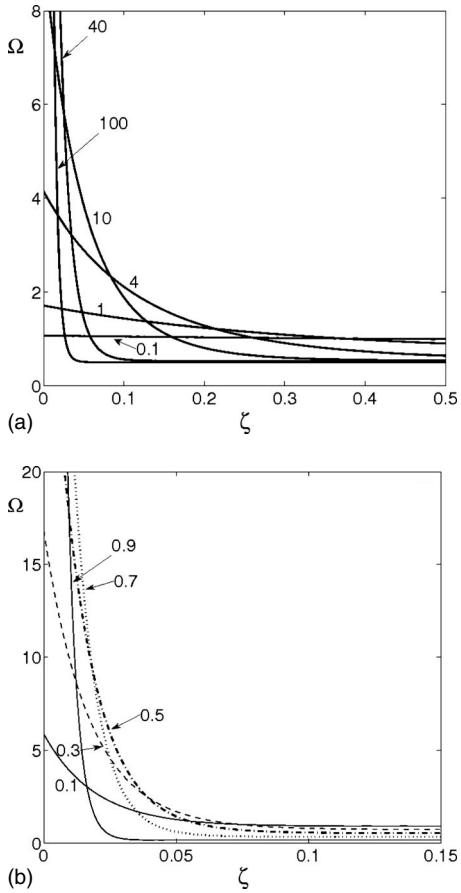

FIG. 2. (a) Ion density profiles for different Peclet values and $S=0.5$, $t/\tau_C=\mathrm{Pe}\tau=0.5$. (b) Ion density profiles for Pe=40 at different values of $[1-S(t)]$, indicated on each curve.

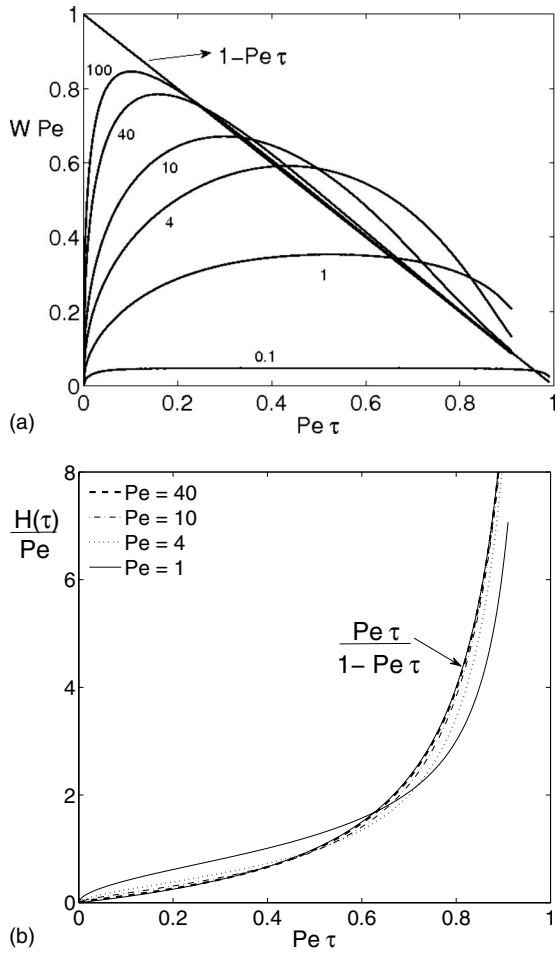

FIG. 3. (a) Peak width $W(\tau)$ for different Peclet numbers as a function of time, where $\mathrm{Pe}\tau=t/\tau_C$. (b) Peak height $H(\tau)$ normalized with Pe vs $\mathrm{Pe}\tau$ for different values of the Peclet number. The solution for $H(\tau)$ given in Eq. (10) is in excellent agreement with the numerical results of the full problem for $\mathrm{Pe}\gg 1$. The curve for Pe=100 is indistinguishable from the theoretical prediction.

tion dominates and the ion distribution is characterized by a narrow region of high salt concentration adjacent to the free surface.

C. Solution for Pe≫1

In Fig. 2(b), we present the time evolution of the ion density profile for Pe=40. We observe that a peak first appears, the concentration profile broadens along the ζ direction, reaches a maximum width and then contracts at later times, while the concentration maximum at the surface $\zeta=0$ increases continuously. Outside of the region of the peak of concentration the ion density is nearly uniform and the effective density Ω simply decreases in time because of the convection of water toward the free surface: $\Omega\simeq 1-\mathrm{Pe}\tau$.

We seek to better understand analytically the mechanisms underlying the time evolution of the peak of the concentration. Consequently, as in Ref. 3, we define the excess density Ω'

$$\Omega'(\zeta,\tau)=\Omega(\zeta,\tau)-(1-\mathrm{Pe}\tau). \tag{6}$$

We characterize the shape of the ion distribution profile by means of the peak height $H(\tau)=\Omega'(0,\tau)$ and the peak width $W(\tau)$, where

$$W(\tau)=\frac{\int_0^1\Omega'(\zeta,\tau)\zeta d\zeta}{\int_0^1\Omega'(\zeta,\tau)d\zeta}. \tag{7}$$

Huinink *et al.*[3] provided analytical results valid at early times, when the concentration distribution evolves diffusively so that the dimensional peak width behaves like $w\approx\sqrt{D^*t}$. They also pointed out that the maximum concentration is instead influenced by the convective flow toward the free surface, which leads to $H\approx\sqrt{\rho^2 j_{\mathrm{cr}}^2 t/(D^*\epsilon^2)}$. We now provide analogous results for later times in the constant evaporation rate regime.

In Fig. 3(a), the numerical results for the time evolution of $W(\tau)$ are reported for various values of the Peclet number. The axes are both scaled with Pe to illustrate scalings that are appropriate for larger Pe (see below). For $\mathrm{Pe}\ll 1$, diffusion tends to spread ions uniformly throughout the sample and, as pointed out by Huinink *et al.*,[3] the peak width remains nearly constant and close to half the sample size. On the contrary, for $\mathrm{Pe}\gg 1$, the peak width is limited by convection and ions are trapped in a region close to $\zeta=0$. Numerical results show that the peak width reaches a maximum and then decreases in time at a constant rate, thus approaching a limit curve.

This behavior is determined by a competition between the convective and diffusive fluxes. In order to corroborate this understanding, we examined the relative magnitude of the four terms in Eq. (5): The first two terms on the right-hand side represent, respectively, these diffusive and convective fluxes, and are, after an initial transient and within the peak region, much larger than the two remaining terms. Outside of the peak region, the time derivative and the term linear in Ω simply express the behavior $\Omega \simeq 1-\mathrm{Pe}\tau$.

By using definition (6) we can rewrite Eq. (5) in terms of the excess density Ω'. Thus, in the neighborhood of the free surface, we make a scaling estimate to obtain an approximate expression for the peak width $W(\tau)$,

$$\frac{\partial^2 \Omega'}{\partial \zeta^2} \simeq \frac{\mathrm{Pe}(\zeta-1)}{1-\mathrm{Pe}\tau}\frac{\partial \Omega'}{\partial \zeta} \Rightarrow W(\tau) \simeq \frac{1-\mathrm{Pe}\tau}{\mathrm{Pe}}. \tag{8}$$

This expression gives the limit curve for $W(\tau)$ to which the numerical results converge for $\mathrm{Pe} \gg 1$ [Fig. 3(a)].

From Eq. (8), it is also possible to obtain an approximate expression for the time evolution of the peak height $H(\tau)$. The integral over the spatial domain of the excess density Ω' can be approximated as the product $H(\tau)W(\tau)$ and, with the chosen nondimensionalization, $\int_0^1 \Omega(\zeta,\tau)d\zeta = 1$. Hence, we have

$$\int_0^1 [\Omega(\zeta,\tau) - (1-\mathrm{Pe}\tau)]d\zeta = \mathrm{Pe}\tau \simeq H(\tau)W(\tau), \tag{9}$$

so that

$$H(\tau) \simeq \frac{\mathrm{Pe}^2\tau}{1-\mathrm{Pe}\tau}. \tag{10}$$

This result is in excellent agreement with the numerical results [see Fig. 3(b)]; even for $\mathrm{Pe}=4$ the analytical approximation is within about 10% of the numerical results.

D. Analytical solution for $\mathrm{Pe} \gg 1$

Using the above ideas, we are now able to obtain an analytical expression for the detailed concentration profile $\Omega(\zeta,\tau)$ for $\mathrm{Pe} \gg 1$ and intermediate times that is in good agreement with the numerical solution of Eq. (5). Indeed, we can assume that, after an initial transient, the concentration $\Omega(\zeta,\tau)$ satisfies a quasisteady differential equation that expresses the balance between convective and diffusive fluxes only. As boundary conditions we impose at $\zeta=1$ the value $\Omega \simeq 1-\mathrm{Pe}\tau$ and at $\zeta=0$ the matching value for the peak height as obtained in Eq. (10). Hence, we consider

$$\frac{\partial^2 \Omega}{\partial \zeta^2} - \frac{\mathrm{Pe}(\zeta-1)}{1-\mathrm{Pe}\tau}\frac{\partial \Omega}{\partial \zeta} = 0,$$

$$\Omega(0,\tau) = 1-\mathrm{Pe}\tau + \frac{\mathrm{Pe}^2\tau}{1-\mathrm{Pe}\tau}, \tag{11}$$

$$\Omega(1,\tau) = 1-\mathrm{Pe}\tau.$$

The solution of this problem is

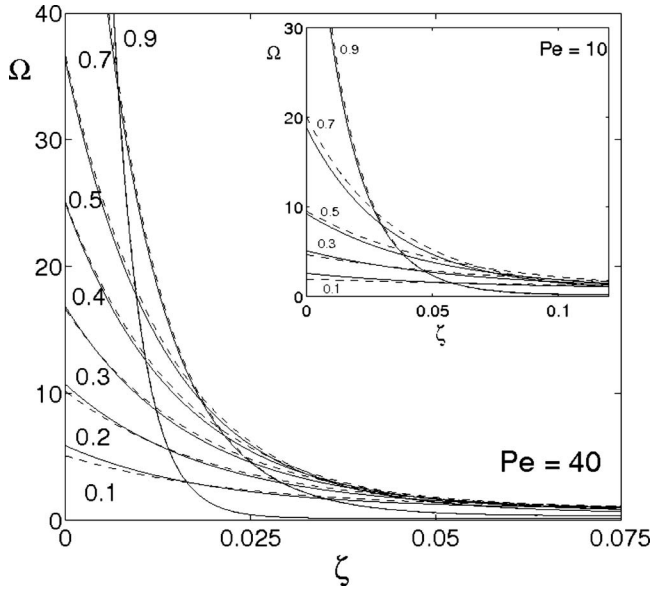

FIG. 4. Ion distribution for $\mathrm{Pe}=40$ and $\mathrm{Pe}=10$ (inset) at different times $0.1 \leqslant \mathrm{Pe}\tau \leqslant 0.9$ during drying. Continuous curves are obtained from the numerical solution of problem (5) and dashed curves represent the solution given in Eq. (12).

$$\Omega(\zeta,\tau) = 1-\mathrm{Pe}\tau + \frac{\mathrm{Pe}^2\tau\,\mathrm{erfi}\left(\frac{\sqrt{\mathrm{Pe}}(\zeta-1)}{\sqrt{2-2\mathrm{Pe}\tau}}\right)}{(\mathrm{Pe}\tau-1)\mathrm{erfi}\left(\frac{\sqrt{\mathrm{Pe}}}{\sqrt{2-2\mathrm{Pe}\tau}}\right)}, \tag{12}$$

where erfi is the imaginary error function.

Figure 4 shows a comparison between the full numerical solution and the analytical solution (12) for $\mathrm{Pe}=40$ and various times. The agreement between the two improves for $\tau \geq 0.3/\mathrm{Pe}$, which [see Fig. 3(a)] is after the peak width $W(\tau)$ has reached its maximum and has started decreasing according to Eq. (8).

E. Cylindrical and spherical geometries

Next we consider two other elementary geometries—cylindrical and spherical—for which basic aspects of drying will be useful to quantify. In both cases, the primary assumption is that the liquid (or saturation) remains uniformly distributed in the sample as the drying occurs, i.e., $S(t)$ only.

First, we consider the cylindrical geometry shown in Fig. 1(b), which is characterized by radius R and height h. We assume that the effect of the top and bottom surfaces on the drying process can be neglected (as is the case when a sample is sealed top and bottom) and that in a median section the liquid phase velocity field and the salt concentration distribution can be assumed to be only functions of the radial coordinate r and time t. In this case, the constant evaporation rate leads to $j_{\mathrm{cr}} = -\frac{1}{2}\rho L\epsilon(dS/dt)$ and $S = 1-(2j_{\mathrm{cr}}/\rho L\epsilon)t$. Thus, the dimensionless form of the ion transport equation is slightly modified from the rectangular case,

$$\frac{\partial \Omega}{\partial \tau} = \frac{1}{\zeta}\frac{\partial}{\partial \zeta}\left(\zeta\frac{\partial \Omega}{\partial \zeta} - \frac{\mathrm{Pe}}{1-2\mathrm{Pe}\tau}\zeta^2\Omega\right), \tag{13}$$

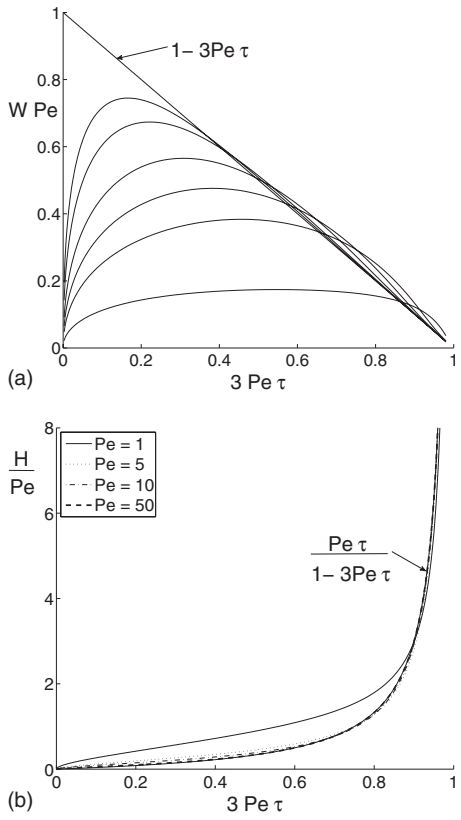

FIG. 5. Spherical geometry. (a) Peak width $W(\tau)$ for different Peclet numbers as a function of time. (b) Peak height $H(\tau)$ normalized with Pe vs time for different values of the Peclet number. The solution for $H(\tau)$ given in Eq. (17) is in excellent agreement with the numerical results of the full problem for $\mathrm{Pe}\gg 1$. The curve for $\mathrm{Pe}=100$ is indistinguishable from the theoretical prediction.

$$\frac{\partial \Omega}{\partial \zeta} - \frac{\mathrm{Pe}}{1-2\mathrm{Pe}\tau}\zeta\Omega = 0 \quad \text{at} \quad \zeta = 0,1, \tag{14}$$

where $\zeta = r/R$, $\tau = tD^*/R^2$, $\Omega = SC/(S_0C_0)$, and $\mathrm{Pe} = Rj_{\mathrm{cr}}/(\rho\epsilon D^*)$.

Since the liquid saturation decreases in time as $S = 1-2\mathrm{Pe}\tau$, and away from the peak region $\Omega \simeq 1-2\mathrm{Pe}\tau$, we introduce the excess density $\Omega'(\zeta,\tau) = \Omega(\zeta,\tau) - (1-2\mathrm{Pe}\tau)$. We again describe the shape of the peak of concentration in terms of the peak height $H(\tau)$ and the peak width $W(\tau)$,

$$W(\tau) = \frac{\int_0^1 \Omega'(\zeta,\tau)\zeta^2 d\zeta}{\int_0^1 \Omega'(\zeta,\tau)\zeta d\zeta}. \tag{15}$$

Following the approach that has been described for the 1D case, we obtain

$$W(\tau) \simeq \frac{1-2\mathrm{Pe}\tau}{\mathrm{Pe}}, \quad H(\tau) \simeq \frac{\mathrm{Pe}^2\tau}{1-2\mathrm{Pe}\tau}. \tag{16}$$

The first expression gives the limit curve for $W(\tau)$ to which we have shown that the numerical solutions to Eq. (13) converge for $\mathrm{Pe}\gg 1$. The second expression in Eq. (16) approximates the time evolution of the peak height and is also in excellent agreement with the numerical solutions of the full problem (13).

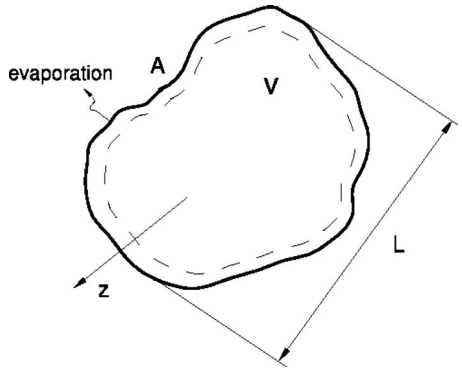

FIG. 6. Schematic of the convective drying of a porous medium of arbitrary shape, sketched here in section. V and A are, respectively, the volume and the area of the surface of the object, while L is its characteristic length scale.

Analogous results can be obtained for a spherical sample [see Fig. 1(c)]. We find that the liquid saturation behaves in time as $S = 1-3\mathrm{Pe}\tau$ and the peak evolution is described by

$$W(\tau) \simeq \frac{1-3\mathrm{Pe}\tau}{\mathrm{Pe}}, \quad H(\tau) \simeq \frac{\mathrm{Pe}^2\tau}{1-3\mathrm{Pe}\tau}. \tag{17}$$

As an example, in Fig. 5(a) the numerical results for the time evolution of $W(\tau)$ for the case of a sphere are reported for various values of the Peclet number, together with the limit curve, given in Eq. (17), to which numerical curves converge for $\mathrm{Pe}\gg 1$. In Fig. 5(b), the time developments of the peak height H obtained from the numerical solutions of the full problem are plotted for different values of the Peclet number and compare well with the approximate expression (17).

Comparing Eqs. (8), (10), (16), and (17) for these idealized geometries in $n=1$, 2, and 3 dimensions, we see that the equations have the same structure. Denoting the surface area A, the volume V, and the characteristic length of the object as L, the typical peak concentration and narrow concentration boundary layer involve the dimensionless ratio AL/V. We next generalize these results to any shape of a drying material.

III. DRYING OF AN ARBITRARY SHAPE OBJECT FOR $\mathrm{Pe}\gg 1$

On the basis of the above results, we now address the problem of drying of an object of arbitrary shape. We consider the constant evaporation rate regime, and hence, assume the evaporation rate to be constant and the liquid saturation to be uniform in the porous medium and function of the time only. In these conditions and for $\mathrm{Pe}\gg 1$, salt tends to accumulate in a narrow region adjacent to the surface where evaporation occurs, while in the rest of the body (see Fig. 6), it remains uniformly distributed and decreases in time because of a purely convective effect. Effectively, the evolution in time of the salt concentration profile depends only weakly on the complexity of the overall geometry and this can be explained by identifying the scale characteristic of the region of maximum concentration, where after an initial transient, $W(\tau) \simeq O(1/\mathrm{Pe})$.

We will proceed here by scaling arguments. We denote by A the surface area, V the volume, and L the characteristic

length of the object. For a given constant drying rate j_{cr}, which depends on the environmental conditions, we have

$$\frac{dS}{dt} \simeq -\frac{AL}{V}\frac{j_{cr}}{\rho\epsilon L}. \tag{18}$$

From this results, it follows that

$$S \simeq 1 - \frac{AL}{V}\frac{j_{cr}}{\rho\epsilon L}t, \tag{19}$$

where AL/V represents the dimensionless ratio between the area of the evaporative surface and the volume of the porous medium. Moreover, from the mass balance equation for the liquid phase, $\nabla\cdot\mathbf{u}=-(dS/dt)/S$, we obtain the characteristic velocity distribution

$$u \simeq -\frac{L}{nS}\frac{dS}{dt}, \tag{20}$$

where n is the dimension of the problem, as used previously. If we assume for simplicity that both the solution density and the medium porosity are constant, the equation for salt transport in the liquid phase can be written in terms of the ion concentration SC as

$$\frac{\partial SC}{\partial t} = D^*\nabla^2(SC) - SC\,\nabla\cdot\mathbf{u} - \mathbf{u}\cdot\nabla(SC). \tag{21}$$

We introduce the usual time scale L^2/D^*, length scale L, and the dimensionless parameter $\mathrm{Pe}=Lj_{cr}/(\rho\epsilon D^*)$. We also define the dimensionless salt concentration per volume of pore spaces Ω in terms of the initial salt concentration.

We expect that away from a narrow region near the surface, the salt concentration is nearly uniform and $\Omega\simeq 1-(AL/V)\mathrm{Pe}\tau$. Near the surface, after an initial transient, the evolution of the ion distribution is determined by a competition between convective and diffusive effects. Moreover, while the gradient of velocity can approximately be considered constant over a scale L, the gradient of salt concentration is nearly zero in the inner part of the porous media and rapidly (exponentially) increases near the surface. Thus, we introduce N orthogonal to the surface, and obtain an approximate expression for the peak width $W(\tau)$ by balancing diffusion and advection,

$$\frac{\partial^2\Omega'}{\partial N^2} \simeq \frac{(AL/V)}{n}\frac{\mathrm{Pe}}{1-(AL/V)\mathrm{Pe}\tau}\frac{\partial\Omega'}{\partial N} \Rightarrow W(\tau)$$
$$\simeq \frac{n}{(AL/V)}\frac{1-(AL/V)\mathrm{Pe}\tau}{\mathrm{Pe}}. \tag{22}$$

Also, similar to the 1D case, we can obtain an approximate expression for the time evolution of the peak height $H(\tau)$. We have

$$\int_V \{\Omega(\mathbf{x},\tau) - [1-(AL/V)\mathrm{Pe}\tau]\}dV$$
$$= \frac{(AL/V)}{n}\mathrm{Pe}\tau \simeq H(\tau)W(\tau), \tag{23}$$

so that

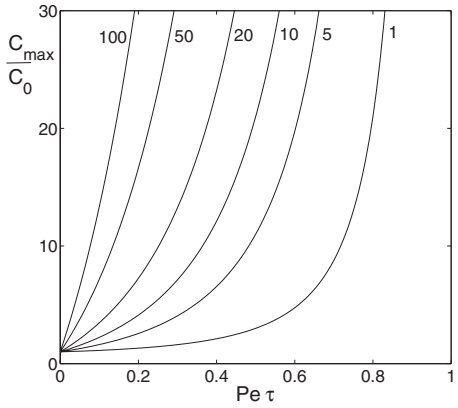

FIG. 7. Time dependent ion concentration at $\zeta=0$ for the geometry in Fig. 1(a) for several values of the Peclet number. The curve for Pe=1 should be interpreted with caution since it is at the limits of applicability of the assumptions in the theory.

$$H(\tau) \simeq \frac{(AL/V)^2}{n^2}\frac{\mathrm{Pe}^2\tau}{1-(AL/V)\mathrm{Pe}\tau}. \tag{24}$$

Thus, the functional forms for the estimate of the width of the narrow high salt region (22) and of the peak concentration (24) generalize the high Peclet number results for the constant rate period to objects of arbitrary shape.

IV. CONCLUSIONS

In conclusion, we have used the 1D model of Huinink *et al.*[3] to study analytically the ion distribution adjacent to a free surface where evaporation occurs. Specifically, for the constant evaporation rate regime, we have focused on time scales such that the convective and diffusive fluxes approximately balance. For the three different 1D cases, rectangular, circular, and spherical, that have been analyzed the analytical expressions for the time dependence of the maximum ion concentration and the typical width of the higher concentrations region are in excellent agreement with the full numerical solutions. In particular, the results indicate the role of the dimensionless surface area to volume ratio, AL/V, which is also identified in our high Peclet number characterization of the drying of arbitrary shapes.

With these results we can learn more about possible salt precipitation at surfaces. In particular, Eq. (10), or, equivalently, Eqs. (16), (17), and (24), for the peak concentration $H(\tau)$ can be used to estimate the time and/or conditions that lead to efflorescence, which refers to the visible appearance of crystal precipitates at the surface. For example, for the geometry in Fig. 1(a), for an initial liquid saturation S_0 and salt concentration C_0, as $\Omega=SC/S_0C_0$, we obtain for the maximum concentration C_{max} at the surface where evaporation occurs ($\zeta=0$)

$$C_{max} = S_0C_0\left[1+\frac{\mathrm{Pe}^2\tau}{(1-\mathrm{Pe}\tau)^2}\right]. \tag{25}$$

We expect $\mathrm{Pe}=O(1-500)$ based on estimates of the characteristic length and porosity of a sample, the environment temperature and relative humidity, and the velocity of the air flow in contact with the sample. Moreover, while salt con-

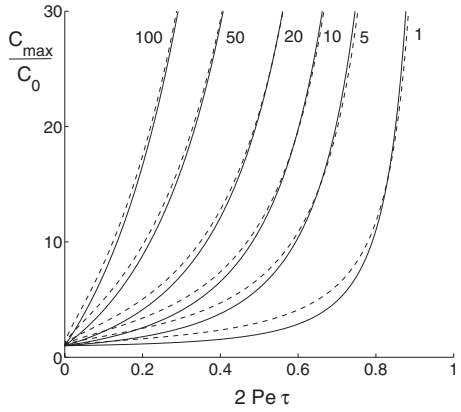

FIG. 8. Time dependent ion concentration at $\zeta = r/R = 1$ for the geometry in Fig. 1(b) for several values of the Peclet number. Continuous lines represent the solution given in Eq. (26), dashed lines the results obtained by solving numerically problem (14). The curve for Pe=1 should be interpreted with caution since it is at the limits of applicability of the assumptions in the theory.

centrations in fresh water can be as low as 0.1%, moderately saline water has typical concentrations in the range of 0.3%–1%, and highly saline water concentrations in the range 1%–3.5%. In Fig. 7, the evolution of $C_{\max}/C_0$ is plotted for $S_0=1$ and different values of the Peclet number. These curves make clear quantitatively (Huinink *et al.*[3] previously indicated the results qualitatively) the typical value of the Peclet number needed, for a given concentration of salt in solution C_0, to prevent efflorescence, i.e., to maintain the concentration of salt at the surfaces $C_{\max}$ below its saturation value during the constant rate period ($S \gtrsim 0.3$), after which the liquid front penetrates into the porous media. The response can thus be adjusted by controlling the environmental conditions during drying or altering the porosity of the material.

Similar expressions can be obtained for the cylindrical and spherical geometries, as well for an object of arbitrary shape (we have neglected the effect of the local curvature of the surface on the spatial variation of the evaporation rate). For the cylindrical geometry, we plot in Fig. 8 the evolution of $C_{\max}/C_0$ for $S_0=1$ and different values of the Peclet number. Dashed curves provide the results obtained by solving numerically problem (14), and continuous curves represent the expression for $C_{\max}$ which follows from substituting the definition of $H(\tau)$ in Eq. (16),

$$C_{\max} = S_0 C_0 \left[1 + \frac{\mathrm{Pe}^2 \tau}{(1 - 2\mathrm{Pe}\tau)^2} \right]. \tag{26}$$

We thus have obtained descriptions for drying in the constant rate period that focus on the common high Peclet number limit, include various geometries, and link the results to final salt concentrations that could lead to, or prevent, efflorescence.

ACKNOWLEDGMENTS

We thank the Harvard MRSEC (MR-0213805) and Grace Construction Products for support of this research.

[1] S. Ben Nasrallah, O. Damak, H. Ben Dhia, and G. Arnaud, "Transfer de soluté au cours du séchage convectif," Int. J. Heat Mass Transfer **34**, 911 (1991).
[2] N. R. Buenfeld, M. T. Shurafa-Daoudi, and I. M. McLoughlin, in *Chloride Penetration into Concrete, Saint-Rémy-lès-Chevreuse, France (1995)*, edited by L. O. Nilsson and J. P. Ollivier (RILEM, Bagneux, 1995).
[3] H. Huinink, L. Pel, and M. A. Michels, "How ions distribute in a drying porous medium: A simple model," Phys. Fluids **14**, 1389 (2002).
[4] L. Pel, H. Huinink, and K. Kopinga, "Salt transport and crystallization in porous building materials," Magn. Reson. Imaging **21**, 317 (2003).
[5] L. Pel, H. Huinink, K. Kopinga, R. P. J. van Hees, and O. C. G. Adan, "Efflorecence pathway diagram: understanding salt weathering," Constr. Build. Mater. **18**, 309 (2004).
[6] Y. T. Puyate, C. J. Lawrence, N. R. Buenfeld, and I. M. McLoughlin, "Chloride transport models for wick action in concrete at large Peclet number," Phys. Fluids **10**, 566 (1998).
[7] N. Sghaier, M. Prat, and S. Ben Nasrallah, "On ions transport during drying in a porous medium," Transp. Porous Media **67**, 243 (2007).
[8] M. Prat, "Recent advances in pore-scale models for drying of porous media," Chem. Eng. J. **86**, 153 (2002).
[9] J. B. Laurindo and M. Prat, "Numerical and experimental network study of evaporation in capillary viscous media: Phase distribution," Chem. Eng. Sci. **51**, 5171 (1996).
[10] M. Prat and F. Bouleux, "Drying of capillary porous media with stabilized front in two-dimensions," Phys. Rev. E **60**, 5647 (1999).
[11] T. M. Shaw, "Drying as an immiscible displacement process with fluid counterflow," Phys. Rev. Lett. **59**, 1671 (1987).
[12] N. Tsimpanogiannis, Y. C. Yortsos, S. Poulou, N. Kanellopoulos, and A. K. Stubos, "Scaling theory of drying in porous media," Phys. Rev. E **59**, 4353 (1999).
[13] P. Coussot, "Scaling approach of the convective drying of a porous medium," Eur. Phys. J. B **15**, 557 (2000).
[14] Y. Le Bray and M. Prat, "Three dimensional pore network simulation of drying in capillary porous media," Int. J. Heat Mass Transfer **42**, 4207 (1999).